Polar Science 14 (2017) 9–20

Contents lists available at ScienceDirect

Polar Science

journal homepage: https://www.evise.com/profile/#/JRNL_POLAR/login

Can preferred atmospheric circulation patterns over the North-Atlantic-Eurasian region be associated with arctic sea ice loss?

Berit Crasemann [a], Dörthe Handorf [a, *], Ralf Jaiser [a], Klaus Dethloff [a], Tetsu Nakamura [b], Jinro Ukita [c], Koji Yamazaki [b]

[a] Alfred-Wegener-Institut, Helmholtz-Zentrum für Polar- und Meeresforschung, Potsdam, Germany
[b] Hokkaido University, Sapporo, Japan
[c] Niigata University, Niigata, Japan

ARTICLE INFO

Article history:
Received 19 May 2017
Received in revised form
5 September 2017
Accepted 8 September 2017
Available online 14 September 2017

Keywords:
Atmospheric circulation regimes
Arctic-midlatitude linkages
Cluster analysis

ABSTRACT

In the framework of atmospheric circulation regimes, we study whether the recent Arctic sea ice loss and Arctic Amplification are associated with changes in the frequency of occurrence of preferred atmospheric circulation patterns during the extended winter season from December to March. To determine regimes we applied a cluster analysis to sea-level pressure fields from reanalysis data and output from an atmospheric general circulation model. The specific set up of the two analyzed model simulations for low and high ice conditions allows for attributing differences between the simulations to the prescribed sea ice changes only. The reanalysis data revealed two circulation patterns that occur more frequently for low Arctic sea ice conditions: a Scandinavian blocking in December and January and a negative North Atlantic Oscillation pattern in February and March. An analysis of related patterns of synoptic-scale activity and 2 m temperatures provides a synoptic interpretation of the corresponding large-scale regimes. The regimes that occur more frequently for low sea ice conditions are resembled reasonably well by the model simulations. Based on those results we conclude that the detected changes in the frequency of occurrence of large-scale circulation patterns can be associated with changes in Arctic sea ice conditions.

1. Introduction

Over the last decades, the Arctic sea ice has declined throughout the year, but most strongly in late summer (see e.g. http://www.meereisportal.de/en/seaicetrends/monthly-mean-arctic). In September, the Arctic sea ice has declined by 12% per decade since the beginning of satellite measurements in 1979 (Stroeve et al., 2011). In the same period, the winter temperatures in the Arctic have risen by 1.6K/decade, which is stronger than anywhere else on the Northern Hemisphere (Screen and Simmonds, 2010). The sea ice decline exerts a strong impact on the atmospheric circulation. Low sea ice conditions in autumn often result in cold Eurasian winters, extreme snowfall, strong blockings and a negative phase of the Arctic Oscillation (AO) and North Atlantic Oscillation (NAO) in late winter (e.g. Jaiser et al., 2012; Cohen et al., 2012; Nakamura et al., 2015).

Many studies analyzed the impact of autumn sea ice conditions on the winter circulation. Francis et al. (2009) investigated the dynamical response to the Arctic sea ice loss, which becomes detectable in terms of modifications of Rossby waves and the jet stream. They showed that the reduced sea ice leads to a weakening of the polar jet stream. Rossby waves get higher amplitudes and move slower which favors the development of blockings and extreme weather such as cold air outbreaks at the Eastern Continents (Francis and Vavrus, 2012). Honda et al. (2009) described the excitation of an atmospheric Rossby wave due to heating anomalies over the Barents/Kara Seas (BKS) in November, which strengthens the development of the Siberian high. Studies by Petoukhov and Semenov (2010), Inoue et al. (2012), Mori et al. (2014), and Overland (2016) showed that low sea ice conditions in autumn are linked to a strong Siberian high and cold Eurasian winters. Additional moisture provided from more opened Arctic Ocean leads to increased snow fall over Eurasia in autumn and winter as pointed out by Cohen et al. (2012), Liu et al. (2012), and Wegmann et al. (2015). Vihma (2014) summarized the interrelation between Arctic sea ice and large-scale circulation anomalies, which includes a high over Eurasia, a high over Western and a low over Eastern North America in winter. Overland and Wang (2010) showed that

* Corresponding author.
E-mail address: doerthe.handorf@awi.de (D. Handorf).

http://dx.doi.org/10.1016/j.polar.2017.09.002

the frequency of the Arctic Dipole, a more meridional pattern, appears more often in the 21st century compared to the 20th century which can be linked to the Arctic sea ice reduction.

Among others, Jaiser et al. (2012) pointed out that sea ice changes can impact the dominant pattern of the large-scale extra-tropical circulation, namely the AO. Thereby, low sea ice conditions foster a shift towards the negative phase of the AO. Kim et al. (2014), Nakamura et al. (2015, 2016), and Jaiser et al. (2016) also focused on the modulation of the AO and NAO following Arctic sea ice loss. They confirmed that low sea ice conditions favor a negative AO/NAO phase through coupling with the stratospheric polar vortex.

Most studies analyze the seasonal winter response to low sea ice conditions. The dynamical response, however, varies greatly from month to month (Deser and Phillips, 2009; García-Serrano et al., 2016). Recent studies by e.g. Cohen et al. (2014), Jaiser et al. (2016), Nakamura et al. (2015) propose a temporal evolution of pathways for Arctic-midlatitude linkages from autumn to winter, which requires studying the related processes with higher temporal resolution.

It has long been recognized that the concept of atmospheric circulation regimes is useful in understanding main aspects of the low-frequency variability of the extra-tropical atmospheric circulation. Today it is common to describe this low-frequency variability in terms of a few preferred and recurrent circulation patterns called circulation regimes (see review by Hannachi et al., 2017). Within this conceptual framework, low-frequency variability could arise owing to transitions between distinct atmospheric circulation regimes.

Furthermore, the frequency of occurrence of preferred atmospheric circulation regimes is influenced by the external forcing factors such as other components of the climate system (e.g., the forcing of large-scale waves by anomalies of the sea surface temperature in the tropics; see Hoskins and Karoly, 1981) or anthropogenic forcing. Palmer (1993, 1999) introduced a dynamical paradigm for climate change. According to this paradigm, a weak external forcing does not change the structure and number of atmospheric regimes, but instead changes the frequency of occurrence of the regimes. This determines, at least partly, the time-mean response of the atmospheric flow to the external forcing. On the other hand, strong external forcing factors can lead to changes in the number and structure of circulation regimes as proven in several studies, e.g. by Kageyama et al. (1999) and Handorf et al. (2009).

Stephenson et al. (2004) and Hannachi et al. (2017) reviewed many studies that have shown the division of the Northern Hemispheric boreal winter flow into two to six preferred circulation regimes under present-day conditions based on daily and monthly data. Using the paradigm of circulation regimes, we are going to study whether the strong Arctic sea ice loss in the last decades can act as an additional external forcing to the atmosphere, which influences the frequency of occurrence of the preferred circulation regimes and leads to a more frequent occurrence of particular patterns.

We determine preferred atmospheric circulation patterns based on sea-level pressure (SLP) fields over the North-Atlantic-Eurasian region of the Northern Hemisphere (30° – 90°N, 90°W-90° E) for winter (DJFM) and analyze changes in the frequency of occurrence in association with different Arctic sea ice conditions. The North-Atlantic-Eurasian region was chosen because of the evidence from observational and modelling studies for dynamical pathways and a monthly progression of processes connecting Arctic sea ice anomalies over the BKS in late summer and autumn to cold Eurasia temperatures in mid-to late winter (e.g. Honda et al., 2009; Cohen et al., 2014; Overland et al., 2015). We analyze the related patterns of synoptic-scale activity and 2 m temperatures to characterize the circulation regimes with respect to synoptic-scale processes. We argue for the association with Arctic sea ice changes is reasoned by the comparison of results from reanalysis data with the output from the two atmospheric general circulation model (AGCM) simulations which differ only in terms of the Arctic sea ice conditions. The paper is organized as follows: Section 2 describes the used data sets and model simulations and the regime analysis method. Section 3 explains the results of the regime analysis for reanalysis and model data, whereas Section 4 provides the discussion of the results and completes with conclusion and outlook.

2. Methods

2.1. Data

We make a use of the recent ERA-Interim reanalysis data provided by the ECMWF (Dee et al., 2011). The data is computed at the T255 spectral resolution (approximately 0.75°), while we use interpolated daily output at the 2° horizontal resolution from 1979 to 2014. Based on the Arctic sea ice concentration and the Arctic sea ice index, provided by the National Snow and Ice Data Center (Fetterer and Knowles, 2004), it is possible to divide the ERA-Interim data into high and low sea ice concentration periods as in Jaiser et al. (2016). The high ice period starts in 1979 and ends in winter 1999/2000, whereas the low ice period continues from winter 2000/2001 until 2014. An inspection of the sea ice anomaly maps reveals large sea-ice reductions between the low and high ice period, but with regional differences. In September, sea ice is reduced over the Beaufort, East Siberian, Laptev, Kara and northern Barents Sea, whereas sea-ice retreat is located in the Barents-Kara Sea and the Chukchi Sea/Bering Strait in November, and in the Barents Sea, the Nordic Sea, and the Sea of Okhotsk in January (cf. Fig. 1 in Nakamura et al. (2015) and Fig. 1 in Jaiser et al. (2016)).

The model simulations have been run with the atmospheric general circulation model for Earth Simulator (AFES) with a spectral resolution of T79 described by Nakamura et al. (2015). They have performed a sensitivity experiment with two perpetual model runs, each with an integration time of 60 years. The first experiment is labeled CNTL and represents high sea ice conditions by using the

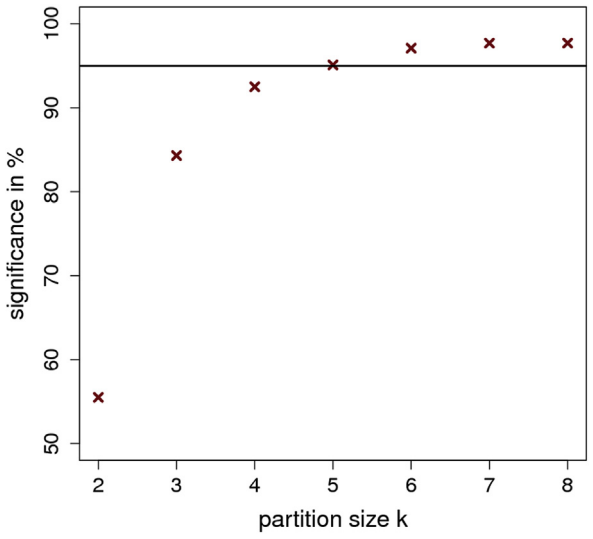

Fig. 1. Significance of the clustering of the ERA-Interim daily SLP fields over the North-Atlantic-Eurasian region for DJFM for k = 2 … 8 clusters. k = 5 is the smallest significant partition size which is significant at the 95% level (black line) and therefore used as cluster size.

mean observed annual cycle of sea ice concentration averaged over 1979–1983 as the lower boundary condition. The prescribed sea-ice conditions have been estimated from the merged Hadley-National Oceanic and Atmospheric Administration (NOAA)/Optimum Interpolation (OI) Sea Surface Temperature (SST) and Sea-Ice Concentration (SIC) data set (Hurrell et al., 2008). Low sea ice conditions are prescribed in the second experiment that is labeled NICE. These are represented by the mean annual cycle of sea ice concentration averaged over 2005–2009. An inspection of the prescribed sea ice anomaly maps between the NICE and CNTL simulation shows the same regional patterns of sea-ice reduction as for the ERA-Interim data (described above), but with larger magnitude (cf. Fig. 1 in Nakamura et al. (2015) and Fig. 1 in Jaiser et al. (2016)). Both experiments use the same mean SST-fields from the early period to focus only on the sea ice changes. A more detailed description of the set-up can be found in Nakamura et al. (2015).

Atmospheric circulation changes between the low and high ice periods in ERA-Interim cannot solely be associated with Arctic sea ice changes because of additional forcing factors. In AFES, sea ice is the only varied parameter between the two model runs. Therefore the response of the atmosphere is directly associated with Arctic sea ice changes. If the differences between the high ice and the low ice period in the reanalysis data are similar to those between the CNTL and the NICE model experiments results, then we attribute the signals to the influence of Arctic sea ice concentration.

2.2. Detection of preferred circulation patterns and changes in the frequency of occurrence

The applied regime analysis method is similar to the one used in Dawson et al. (2012) and Dawson and Palmer (2015). It considers preferred regions of the state space as circulation regimes. These preferred regions are identified by grouping daily fields of SLP anomalies into clusters with similar anomaly patterns.

Our regime analysis is based on daily SLP fields over the North-Atlantic-Eurasian region (30°–90°N, 90°W-90° E) for the 4 winter months (DJFM). We have chosen this region due to the increased evidence for dynamical pathways linking in particular Arctic sea ice anomalies of the BKS in late summer and autumn to cold Eurasia temperatures in mid-to late winter (see Introduction).

First, the SLP anomaly fields have been calculated by subtracting the mean annual cycle at each grid point. For the reanalysis, the mean annual cycle has been calculated over the period 1979–2014, whereas for the model simulations the mean annual cycle has been calculated separately for the CNTL and NICE model runs to take into account the different background states. In order to reduce the dimensionality of the data set, we have applied an empirical orthogonal function (EOF) analysis with ensured equal-area weighting. For the reanalysis data, the EOF analysis and subsequent cluster analysis has been carried out for the full period 1979–2014 covering the high and low ice period. To cover high and low ice period for the analysis of the model data, we applied an EOF analysis to the combined data of the CNTL and NICE runs, resulting in a sample of 120 years of daily data. We selected the five leading EOFs as basis functions to span the reduced state space, where the corresponding Principal Component (PC) time series provide the coordinates of the reduced state space. The EOF patterns and PC time series have not been re-normalized, thus the variance of the corresponding PC time-series is equal to the corresponding eigenvalue. The five leading EOFs explain 40–50% of variance of the SLP anomaly fields. The results of the cluster analysis are not sensitive to the dimension of the reduced state space, which has been tested over the range from 3 to 10 EOFs.

The five leading EOF patterns of ERA-Interim and AFES correlate well with pattern correlation coefficients between 0.84 and 0.94, which are significant at the 95% confidence level by a Student's t-test. Therefore we have analyzed both data sets in their own state spaces instead of using projected patterns.

We decided to use the k-means clustering algorithm for the identification of regimes in a low-dimensional state space (e.g. Michelangeli et al., 1995; Mo and Ghil, 1988). K-means clustering aims to partition all data into a prescribed number of k clusters, with the requirement of maximizing the ratio of variance between the cluster centroids and the average of the within-cluster variance. Standard iterative algorithms are provided for solving this optimization problem. The R package *kmeans* (R Core Team, 2012) is applied here. We performed 100 iterations starting from 100 random initial partitions to ensure the finding of the optimal solution of the maximization problem.

We tested the null hypothesis of the non-existence of regimes with the same approach as in Straus et al. (2007), Dawson et al. (2012), and Dawson and Palmer (2015). The null hypothesis would result in a multi-normal distribution of the probability density function (pdf) of the underlying state space. In order to test this null hypothesis, Monte Carlo simulations were performed. 500 random quintuples of Pseudo-PC time series have been simulated with the same values for the mean, variance, skewness and lag-one autocorrelation as the original PC time series. Then, the corresponding k-means cluster partitions have been calculated for the simulated quintuples, where the number of clusters has varied between 2 and 8. Significance has been estimated by comparing the estimates of the maximized ratio of variance between the cluster centroids and the average of the within-cluster variance for each simulated data set with the ratio of variance of the original data set. The 95% significance level indicates that 95% of the simulated data sets have a lower variance ratio than the original data, and thus, the variance ratio of the original data shows significant deviations from the variance ratio obtained from data with a multi-normal pdf. The result of this estimate of significance for the clustering of the ERA-Interim daily SLP fields over the North-Atlantic-Eurasian region for DJFM for $k = 2 \ldots 8$ clusters is shown in Fig. 1. Since $k = 5$ is the smallest partition size which is significant at the 95% level, we prescribe the number of clusters as $k = 5$ throughout this study and treated these clusters as atmospheric regimes.

One drawback of k-means clustering is the necessity to prescribe the number of clusters k as an input parameter, which leads to a discussion on whether this method is able to determine the correct number of clusters in a data set (see Christiansen, 2007). But in the same line with the arguments given by Dawson and Palmer (2015), we apply the k-means clustering in order to search for non-Gaussian structures which are identified as regimes. The detected regimes are used to compare the reanalysis and AGCM data, and the concerns about the sufficient number of clusters can be regarded as less relevant.

In order to detect changes in the relative frequency of occurrence of the regimes with respect to the high/low ice periods we calculated histograms for each period. A significance test has been performed to search for regimes which occur significantly more often for low ice conditions. This is achieved by considering the time series describing the occurrence of regimes as a vector with elements $x_i \in \{1,2,3,4,5\}$. 1000 bootstrap replicates of this time series have been generated. For each replicate, a histogram has been calculated for the high and low ice period. Next the corresponding difference of the relative frequency between the low and high ice period of the occurrence of each regime has been determined. If no more than 50 out of the 1000 replicates showed a difference larger than the difference in the relative frequency of occurrence of the original occurrence time series, we detected a significant difference at the 95% level. Boxplots for the distribution

of the differences in the relative frequency of occurrence for the replicates together with the difference values of the original time series have been generated and can be found in the Supplementary Figs. S5 and S6.

2.3. Calculation of large-scale patterns and related synoptic patterns

The calculation of clusters has been performed for the 36 years long ERA-Interim period from 1979 to 2014 with 21 years high ice conditions (1979–1999/2000) and 15 years low ice conditions (2000–2014) as well as for the 120 years AFES simulations including 60 years high ice conditions (CNTL) and 60 years low ice conditions (NICE) in the 5-dimensional reduced state space. The respective 5 leading PCs provide the coordinates of the reduced state space. Whereas the cluster analysis has been performed over the four winter months DJFM to have sample sizes large enough to obtain statistically significant partitions, the cluster occupation frequencies have been determined for each month separately. This approach allows investigating which preferred circulation pattern occurred more frequently in different months during high or low ice conditions.

In the following, the preferred large-scale circulation patterns in terms of SLP and the related fields of synoptic-scale activity and 2 m temperature are shown as anomaly fields, defined by deviations from the monthly climatological mean fields of ERA-Interim and AFES, respectively.

The corresponding large-scale circulation patterns are reconstructed from the 5-dimensional coordinate vectors of the cluster centroids. These patterns are very similar to those obtained by calculating composites in the full space of SLP anomaly fields over those points that belong to the respective cluster.

By applying this compositing method, anomaly patterns of 2 m temperature and synoptic-scale activity have been calculated, which are related to the five preferred large-scale patterns. The significance of the anomalous signals for temperature has been determined with a Student's t-test. Synoptic-scale activity is defined as the standard deviation of the 2–6 days bandpass-filtered mean sea level pressure from the daily data (Blackmon, 1976). Since synoptic-scale activity is based on variances, significance has been determined with an F-Test. We calculated a significance level by asking whether or not the five related synoptic-scale activity and temperature patterns differ from each other. If a 99% significance level is reached, the signals in the anomaly maps are highlighted with black dots.

3. Results

In the following, we study the preferred planetary-scale patterns over the North-Atlantic-Eurasian sector of the Northern Hemisphere for the extended winter season December, January, February and March and analyze individually those patterns that occur more frequently during low Arctic sea ice conditions in each month. Further, we relate the large-scale circulation patterns to synoptic-scale activity and 2 m temperature patterns. This analysis is done for ERA-Interim and compared to AFES with respect to Arctic sea ice conditions.

The five preferred large-scale patterns determined for the extended winter season for ERA-Interim (ERA-I) and AFES are shown in Fig. 2, left column for ERA-I, right column for AFES. The ERA-Interim clusters are ordered by their levels of absolute occurrence. For the sake of easier comparisons, the AFES clusters are reordered so as to follow the order of the ERA-Interim clusters. ERA-Interim and AFES almost have the same large-scale patterns resembling a positive NAO signal (NAO+); a high pressure system centered over Scandinavia and extended towards northern Siberia (SCA); a pattern with a low pressure system over the North Atlantic and Europe and surrounded by positive anomalies in ERA-Interim (ATL-); a negative NAO signal (NAO-); and a west-east dipole structure with positive pressure anomalies over the Atlantic and Greenland and negative anomalies over Europe and the BKS (DIPOL).

Based on the histogram with the relative frequency of occurrence for ERA-Interim and AFES (Fig. 3a and b), we find that the SCA pattern occurs more frequently in December and January for low sea ice conditions compared with high sea ice conditions. The difference of the relative frequency of occurrence in December for low ice conditions is 8 percentage points for ERA-Interim, while the occurrence for AFES differs only slightly with the same sign. In January the difference is still larger for ERA-Interim with 9 percentage points versus an almost equal occurrence for AFES. Based on the significance test described in section 2.2, the SCA pattern occurs significantly (at 95% level) more frequent in December and January for low sea ice conditions in the reanalysis data, and significantly more frequent in December for low sea ice conditions in the model simulation (see also Supplementary Figs. 5 and 6). Additionally, the ATL-pattern also shows more frequent occurrence in January under low ice conditions for ERA-Interim (non-significant difference) and AFES (significant difference).

In February and March, the NAO- pattern appears more frequently for low sea ice conditions. Here, the differences of the relative frequencies of occurrence between low and high ice conditions are large and statistically significant for both ERA-Interim and AFES. In February, there is a difference of 8 percentage points for ERA-Interim and 3 percentage points for AFES. In March, ERA-Interim shows a difference of 10 percentage points and AFES of 3 percentage points. Additionally, the AFES analysis reveals more frequent occurrence of the NAO + patterns in February (significant) and March (non-significant) with a change in relative frequency by 3 and 2 percentage points, respectively. This indicates a stronger dominance of the variability pattern of the NAO due to the external forcing following the reduced sea-ice in AFES.

Below, we analyze the related patterns for synoptic-scale activity and surface air temperature (SAT) for each month separately if the large-scale regime occurs more frequently for low ice conditions. Accordingly, we show the patterns related to SCA in December and January and to NAO- in February and March. The scope is the association of the large-scale circulation regimes with the synoptic situation. We will concentrate on the signals that occur simultaneously in ERA-Interim and AFES in order to show the connection of the patterns with the decrease of Arctic sea ice conditions.

3.1. December/January

The SCA pattern in December and January is associated with an SAT anomaly pattern similar to the Warm Arctic-Cold Siberia pattern (WACS, Inoue et al., 2012). Strong negative temperature anomalies up to -8K over central Europe and Siberia appear in December (Fig. 4a). Positive temperature anomalies between 1 and 6K exist over the Greenland Sea and over the Barents, Kara and Laptev Seas in ERA-Interim and AFES with the extension towards the East Siberian Sea in AFES only. Notably, a pronounced anomaly of 8K is found over Eastern Greenland and Svalbard in both data sets. All these anomalies are statistically significant.

The positive temperature anomalies over the Arctic coincide with an enhanced Atlantic storm track (Fig. 4b), which is shifted further northwards compared to its climatological position. The positive anomaly of 1.5hPa in synoptic-scale activity appears between Newfoundland and the Barents Sea, which is roughly a 30%

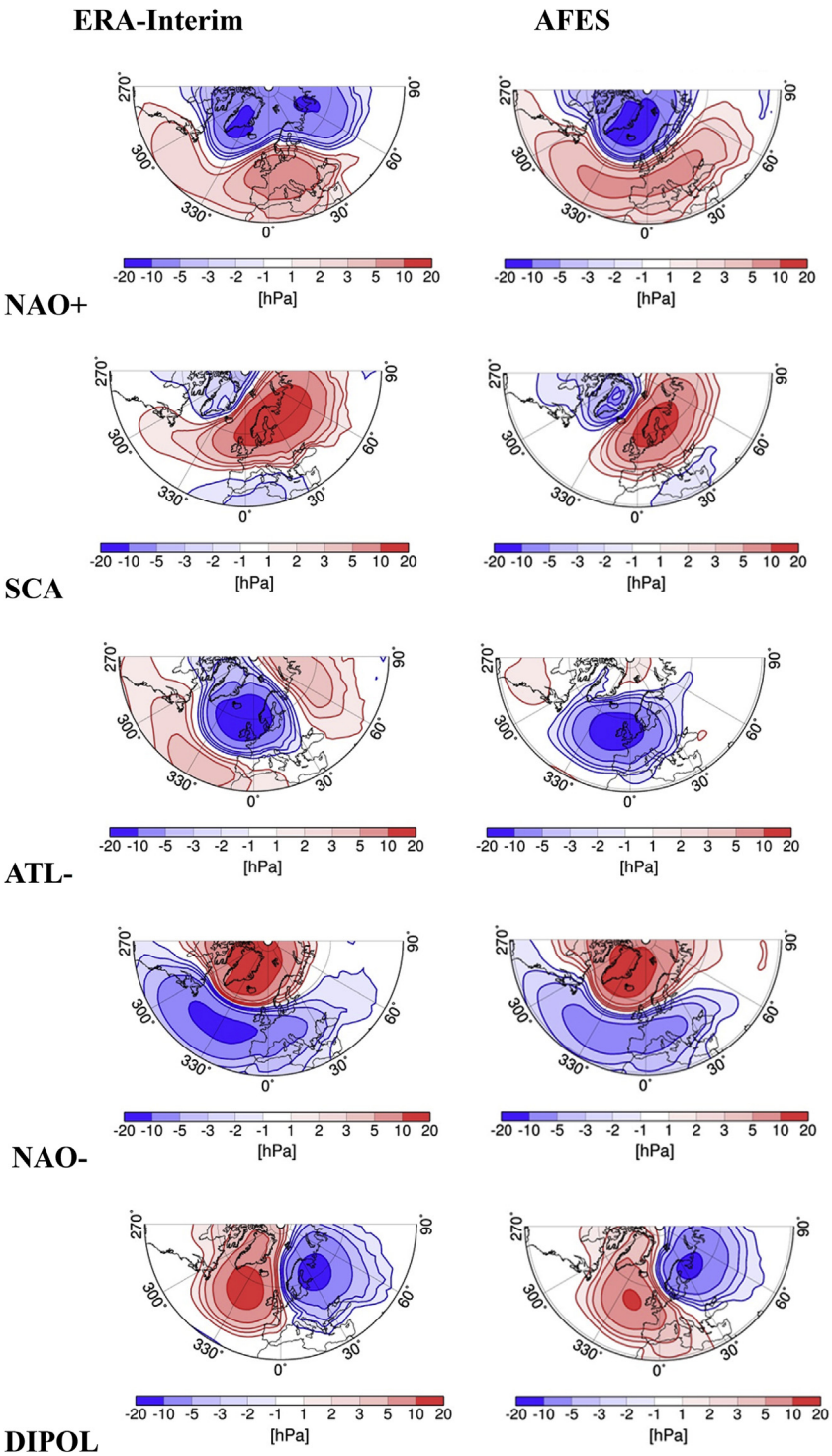

Fig. 2. SLP anomalies of the five preferred large-scale patterns obtained by a cluster analysis, left column for ERA-Interim, right column for AFES. The ERA-Interim clusters are ordered by their absolute frequency of occurrence. For the sake of easier comparisons, the AFES clusters are re-ordered so as to follow the order of the ERA-Interim clusters.

increase compared to the climatological values between 4 and 6hPa (see Suppl. Fig. S3). This implies that more cyclones reach the Arctic when the large-scale pattern is characterized by the strengthened high pressure anomaly over Scandinavia and Siberia. In contrast, the synoptic-scale activity over Europe is reduced by the same magnitude due to the northward shifted storm track. These anomalies are significant in both ERA-Interim and AFES.

In January, the SCA patterns as well as the related anomaly patterns of 2 m-temperature and synoptic-scale activity are similar to their counterparts in December. The main differences compared to December are stronger negative temperature anomalies of 2K over Eastern Europe and Siberia and a larger area with positive temperature anomalies over Svalbard (Fig. 5a). The anomalies of the synoptic-scale activity over the Arctic display a weaker reduction over Northern Europe (Fig. 5b).

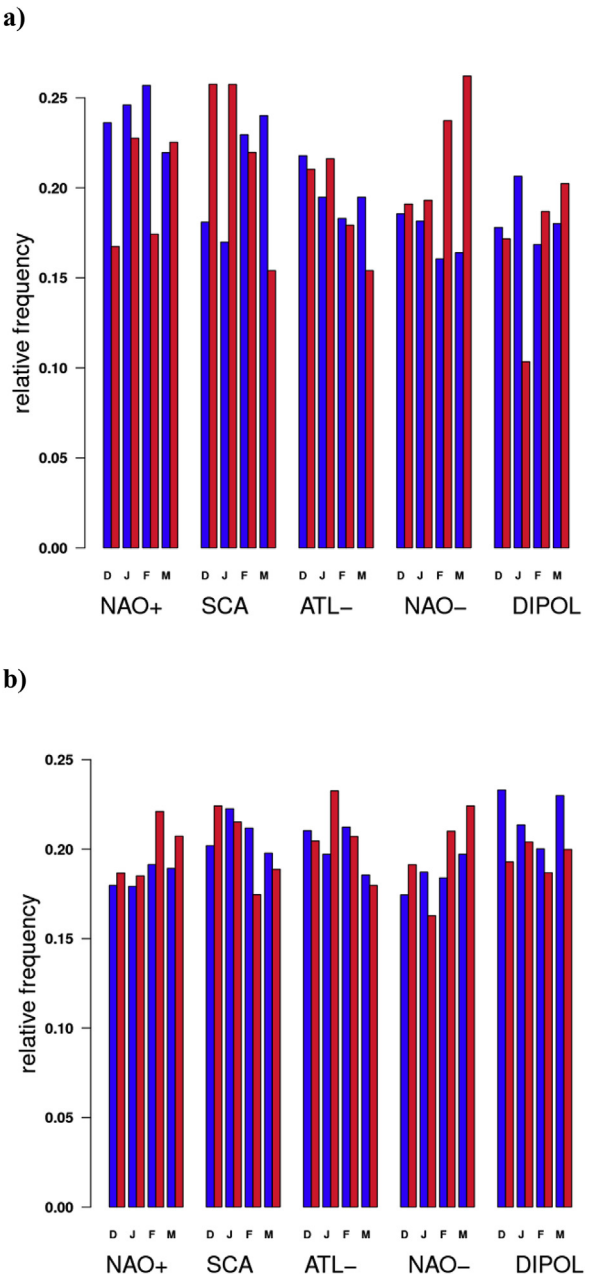

Fig. 3. Relative frequency of occurrence of the five clusters for December, January, February and March with respect to the Arctic sea ice conditions for a) ERA-Interim and b) AFES. Each blueish bar gives the relative frequency of occurrence for high ice conditions and each reddish bar for low ice conditions. NAO+, SCA, ATL-, NAO- and DIPOL belong to the clusters displayed in Fig. 2.

3.2. February/March

In February, the NAO- pattern, which occurs more frequently for low sea ice conditions, is characterized by positive sea level pressure anomalies of 15hPa over the region between Island and Greenland and negative anomalies of the same magnitude over the South Atlantic and middle Europe. These circulation anomalies are related to positive temperature anomalies of up to 6K over Newfoundland and Greenland and 3K over the Chukchi Sea and Bering Strait. Negative anomalies of up to -3K occur over Alaska and Canada as well as up to -6K over Northern and middle Europe and Siberia (Fig. 6a).

A consistent picture emerges in synoptic-scale activity showing a southward shift of the Atlantic storm track resulting in negative anomalies of 2hPa over the North Atlantic and BKS. An increase of storm activity appears over the South Atlantic, Southern Europe and Russia (Fig. 6b).

In March, the NAO- pattern occurs more frequently for low sea ice conditions comparable to the situation in February. The temperature anomalies in March resemble to the anomalies in February (Fig. 7a). Also, the anomalies for the synoptic-scale activity are similar to the signals in February in the corresponding regions in ERA-Interim and AFES with a strong decrease of cyclonic activity over the North Atlantic and an increase over the South Atlantic (Fig. 7b).

4. Discussion

Our analysis revealed that there are two preferred large-scale circulation patterns in the extended winter season in the Northern Hemisphere, which occur more frequently during low Arctic sea ice conditions both in ERA-Interim reanalysis and the AFES model simulations. During the low Arctic sea ice conditions, there is a characteristic evolution of the pattern of sea-ice retreat from autumn to winter with sea-ice decline over the Barents-Kara Sea in all months whereas sea ice retreat over the Beaufort, East Siberian, and Laptev Sea persists only until October (cf. Yang et al. (2016), Fig. 1 in Nakamura et al. (2015) and Fig. 1 in Jaiser et al. (2016)).

We concentrate our discussion on major large scale circulation changes that occur in consecutive months. In line with this, we found the preferred occurrence of the SCA pattern with a strong blocking centered over Scandinavia and extending to northern Eurasia in December and January. In February and March, the negative phase of the NAO appears as the preferred pattern.

The preferred pattern of the blocking with its center over Scandinavia bears similarity with blocking patterns called the Eurasian pattern type 1 (Barnston and Livezey, 1987), the Scandinavian pattern (Bueh and Nakamura, 2007), the Russian pattern (Smoliak and Wallace, 2015) or the Ural-Siberian blocking (Cheung et al., 2012). The center of the SCA pattern extends over the two major Eurasian blocking formation centers over Scandinavia (~20°–30°E) and upstream of the Ural Mountains (~50°–60°E) as detected by Cheung et al. (2013). The associated SAT anomaly pattern resembles the WACS pattern introduced by Inoue et al. (2012).

The preferred appearance of Eurasian blockings with its center over Scandinavia in December and January may result from different processes. Compared with high ice conditions, low sea ice conditions induce a delayed refreezing of the Arctic Ocean in October and November and additional heat release to the lower atmosphere over the Arctic Ocean. This extra amount of heat reduces the atmospheric vertical static stability and leads to amplified baroclinic synoptic systems over the Arctic (Jaiser et al., 2012; Semmler et al., 2016). In a general dynamic view, the anomalous transient eddy forcing by the amplified baroclinic systems may force planetary waves (Jaiser et al., 2012) and impact the onset and maintenance of blockings downstream of areas with significant sea-ice retreat.

Several studies relate preceding or instantaneous anomalous sea-ice conditions to the emergence of the enhanced appearance of blockings with its center over Scandinavia and northern Eurasia in December and January. In particular, Inoue et al. (2012), Luo et al. (2016), Sato et al. (2014) and Jung et al. (2017) emphasize the association between the instantaneous sea-ice changes in the BKS and blocking patterns over Scandinavia and the Ural in early winter (October–December, Jung et al., 2017), December (Inoue et al., 2012; Sato et al., 2014) and winter (Luo et al., 2017). In Inoue

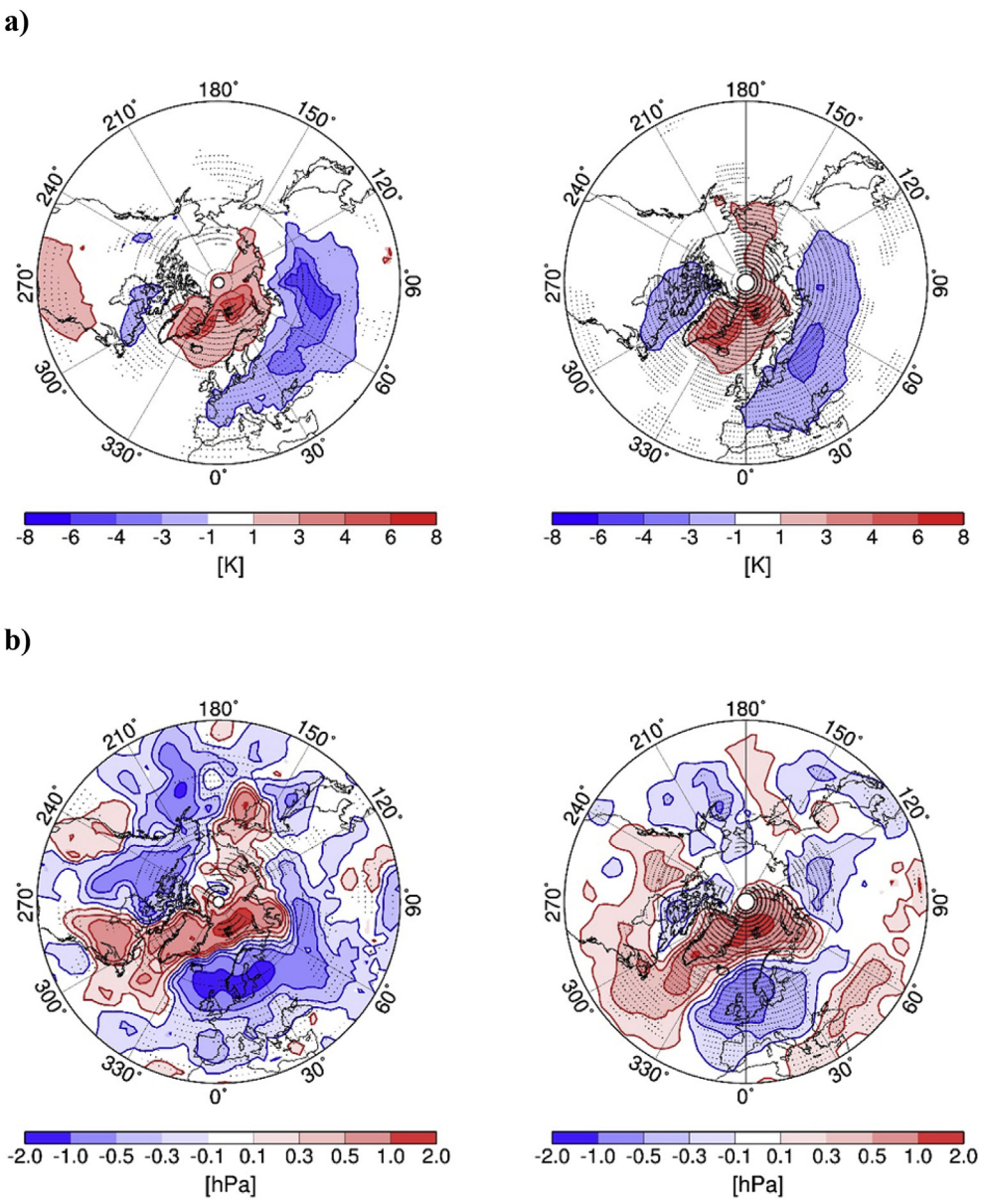

Fig. 4. Anomalies of 2 m-temperatures (a) and synoptic-scale activity (b) for the SCA-pattern in December, left column for ERA-Interim and right column for AFES. Significant anomalies on the 99% level are marked with black dots.

et al. (2012) the maintenance of the anticyclonic anomalies over Scandinavia and the Siberian coast has been related to the fact that for low ice conditions fewer cyclones travel eastward due to lower baroclinicity over the BKS. Model experiments with a simple model carried out by Sato et al. (2014) revealed a local response to the BKS warming in autumn and winter in terms of large-scale anticyclonic anomalies over Scandinavia and northern Eurasia, but without the characteristic WACS pattern. Further model experiments by Sato et al. (2014) and Jung et al. (2017) were performed with simple and general circulation models. They showed that the warming anomalies over the western North Atlantic and subsequent transient eddy forcing over that region provide a wave source for a planetary wave train. This wave train bears similarity with the Scandinavian pattern with anticyclonic anomalies over Scandinavia and northern Eurasia and resembles the WACS pattern.

As suggested by Honda et al. (2009), the persistence of the BKS sea ice anomalies into autumn can provide diabatic forcing for a stationary Rossby wave train in November with anticyclonic anomalies over Northern Eurasia maintained by transient eddy feedback. Due to eastward propagation of this wave train, it could constructively interfere with the Siberian high in December (Honda et al., 2009). The Siberian High is dynamically linked to blocking over Ural-Siberia. In particular the Ural-Siberian blocking formation involves interaction between the Siberian high and an eastward-propagating Rossby wave train (e.g., Takaya and Nakamura, 2005a,b; Cheung et al., 2013). Therefore, a strengthened Siberian high can contribute to the preferred occurrence of the SCA pattern in December and January.

Additionally, the negative BKS sea ice anomalies in October and November provide a moisture source for enhanced Siberian snow cover in these months (Wegmann et al., 2015) Increasing October snow cover extent can precede an SLP pattern with prominent Scandinavian blocking in November to mid-December (Cohen et al., 2014; Gastineau et al., 2017).

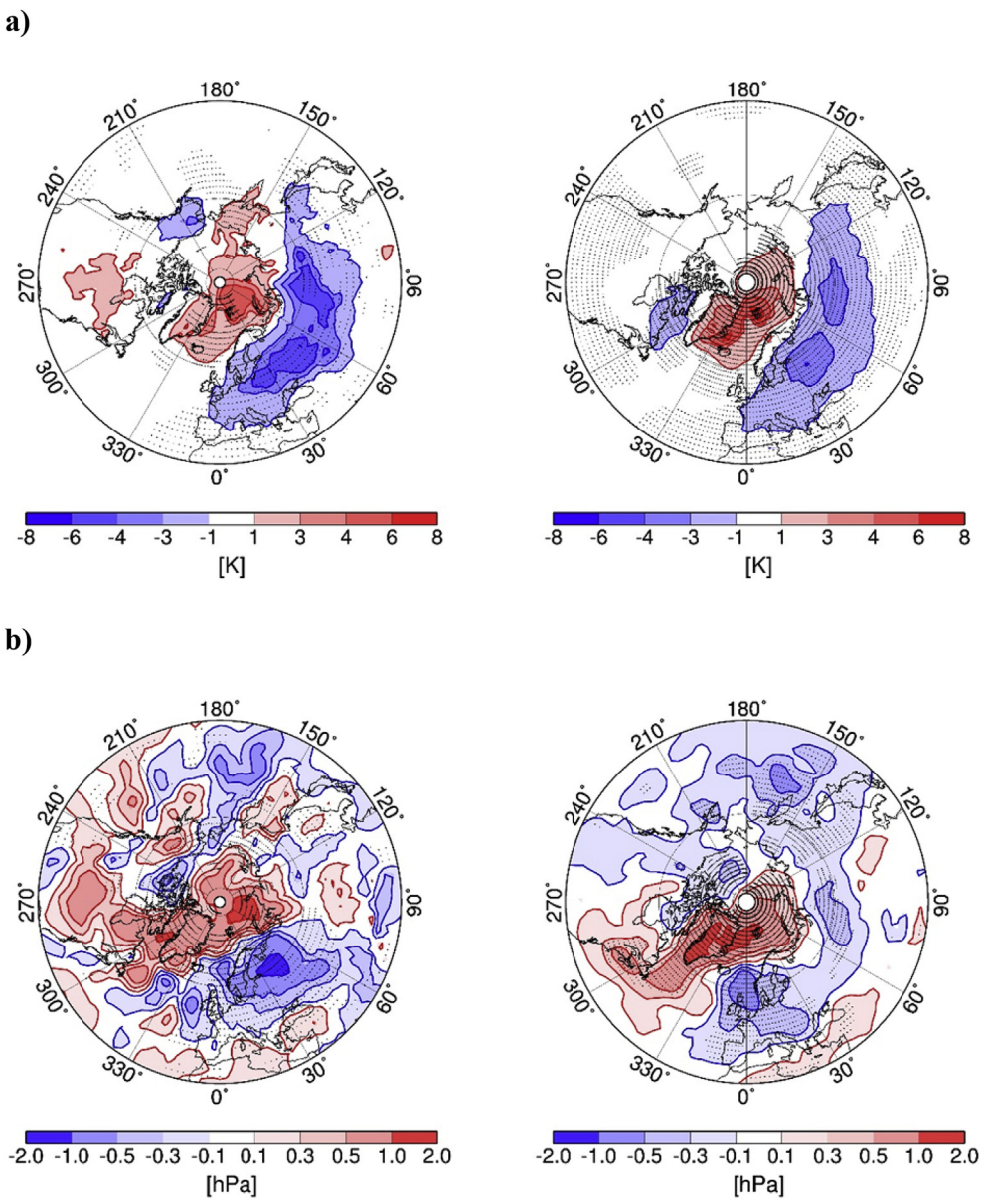

Fig. 5. As Fig. 4, but for January.

Furthermore, the maintenance of the SCA pattern is enhanced by a positive feedback loop. Once the SCA pattern is set-up, strong southerly surface wind anomalies over the BKS occur. Thus, the heat release form the open water to the atmosphere is reinforced, leading to stronger sea-ice reduction and warming over the BKS and reinforcement of the above described local and remote processes for maintaining the SCA pattern.

The blocking pattern over Scandinavia is connected with an increase of synoptic-scale activity over Greenland, the Fram Strait and BKS of up to 2hPa and a decrease close to the blocking center over Europe. Notably, the location of the temperature anomalies, resembling the WACS pattern, coincides with the location of synoptic-scale activity anomalies. Over the North Atlantic, Greenland, Svalbard and the BKS, positive anomalies of up to 8K appear close to the Northern flank of the blocking and negative anomalies of up to -8K in the central regions of the blocking which is associated with the advection of warm mid-latitudinal or cold polar air masses. Over the BKS, positive anomalies are potentially related to enhanced turbulent heat fluxes from the ocean during low ice conditions (Alexander et al., 2004).

In January, the synoptic patterns do not dramatically change compared to December. An intensification of positive temperature anomalies is found over the Svalbard region. This is in accordance with a recent study by Maturilli and Kayser (2016) which showed from long-term radiosounding measurements that the warming over Svalbard is most prominent in January and stretches across the whole tropospheric column. They also argue that this warming is due to circulation changes and preferred occurrence of circulation patterns that transport warm Atlantic air into the Arctic. The synoptic-scale activity anomalies strongly supports their arguments, that for low ice conditions the Atlantic storm track extends further into the Artic and the cyclonic activity is enhanced over Greenland and Svalbard with positive temperature anomalies there.

In January, the more frequent occurrence of the large-scale pattern with the blocking over Scandinavia for low Arctic sea ice

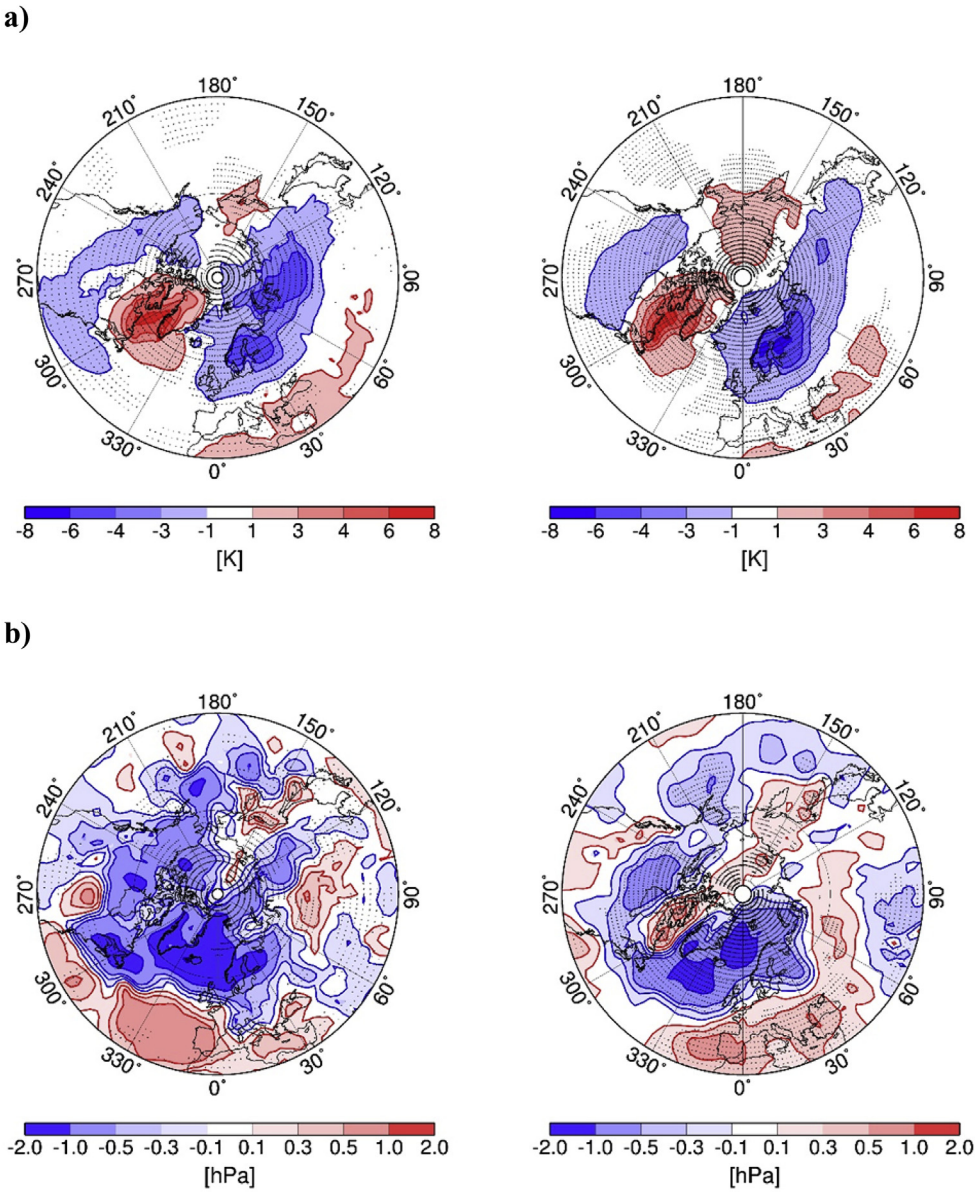

Fig. 6. Anomalies of 2 m-temperatures (a) and synoptic-scale activity (b) for the negative NAO pattern (NAO-) in February, left column for ERA-Interim and right column for AFES. Significant anomalies on the 99% level are marked with black dots.

conditions is detectable in ERA-Interim, whereas no frequency changes have been detected in the AFES simulations. The studies by Honda et al. (2009), Takaya and Nakamura (2005a,b), Cheung et al. (2013), Inoue et al. (2012), Luo et al. (2016), Sato et al. (2014) and Jung et al. (2017) suggest that the preferred occurrence of the SCA regime in December and January are influenced by the local direct response to the sea-ice retreat and warming over the BKS, by the remote response to Rossby wave sources over the Gulf stream region and over the BKS and by synoptic-planetary wave interaction processes. From the AFES sensitivity experiment we cannot derive an influence of the Gulf Stream region, due to the constant SST. This leads to the conclusion that the other two processes are strong enough to generate the Scandinavian blocking pattern at least in December. While the effect of sea ice is directly addressed by our analysis through the AFES sensitivity experiment, the remote response to Rossby wave sources outside the Arctic region and the role of synoptic-planetary wave interaction processes and its representation in models needs to be investigated in future studies.

In February, another preferred circulation pattern characterized by a negative phase of the NAO appears more frequently following low Arctic sea ice conditions in ERA-Interim and AFES. As a possible mechanism, Nakamura et al. (2015, 2016) and Jaiser et al. (2016) suggested a stratospheric pathway, in which vertically propagating waves in early winter interact with the stratospheric polar vortex and weaken it. This leads to positive temperature and negative zonal wind anomalies in the vortex. These anomalous signals propagate downward into the troposphere and favor a negative phase of the NAO in February and March. The more frequent occurrence of the SCA in the preceding period of December and January can initiate and strengthen this stratospheric pathway. When considering the SCA-related anomaly patterns of 2 m temperature (Figs. 4 and 5) and their climatologies (Supplementary Figs. S1 and S2), we detect an intensification of the heat contrast between the warm ocean (Atlantic side of the Arctic Ocean) and the cold continent (especially in Siberia). As an additional effect, the intensified land-sea heat contrast has the potential

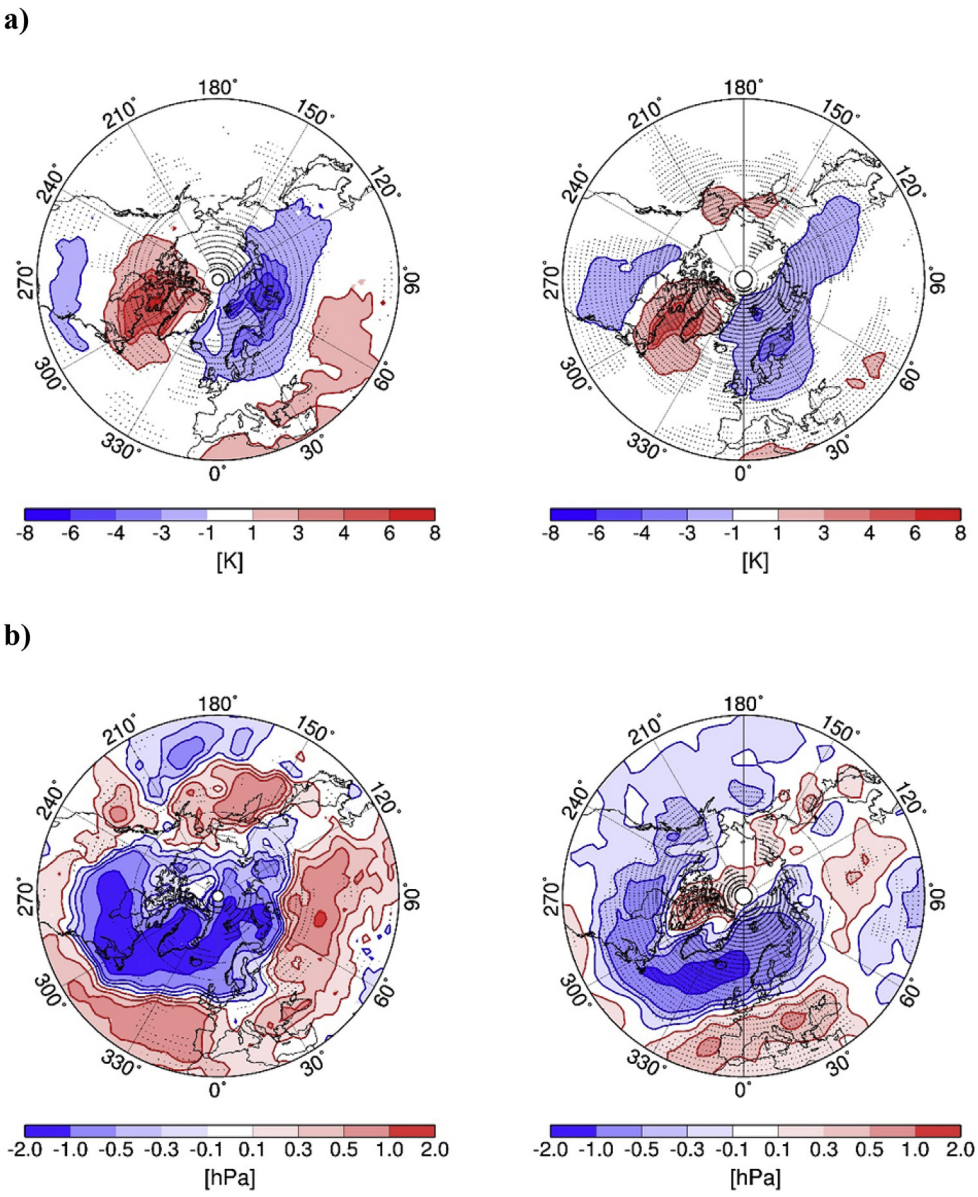

Fig. 7. As Fig. 6, but for March.

to cause an intensified amplification of planetary-scale waves, which is preferable to disturb the stratospheric polar vortex.

The stratospheric pathway can also be initiated and strengthened by increased Siberian snow cover (Cohen et al., 2007; Gastineau et al., 2017). As suggested by Cohen et al. (2007), enhanced snow cover in particular in October is related to enhanced upward propagating planetary waves in late fall and early winter leading to stratospheric warming and to a negative Arctic Oscillation response in January. Gastineau et al. (2017) confirmed that snow cover anomalies in November revealing a dipolar structure with negative anomalies over eastern Europe and positive anomalies over eastern Siberia precede a negative phase of the Arctic Oscillation one and two months later. The study by Orsolini et al. (2016) confirmed the role of the snow-initiated stratospheric pathway for the maintenance of a pre-existing negative NAO phase in early and mid-winter.

In our analysis, this December/January snow response did not manifest as preferred occurrence of the NAO- pattern in December/January. Nevertheless, the early winter disturbances of the stratospheric vortex due to the snow impact could act as a preconditioning of the stratospheric vortex. This enable vertically propagating planetary waves forced by processes related to sea-ice reduction in early and mid-winter to further weaken the stratospheric polar vortex. The downward propagation of these stronger anomalous signals into the troposphere favors the negative phase of the NAO in February and March.

In February, the NAO- pattern is related to negative temperature anomalies of up to -6K over Scandinavia and Northern Siberia. Negative anomalies of up to -3K also exist over Alaska, Canada, the Northeast Atlantic and Eastern Siberia. These negative temperature anomalies result from the weakened zonal flow and less advection of Atlantic air masses. The maximum positive temperature anomalies of up to 4K over the Baffin Bay are an outcome of the reduced zonal flow and likely linked to diabatic heating changes. The positive temperature anomalies of up to 3K over the Chukchi Sea are also due to a reduced zonal flow and weaker advection of cold

Siberian air masses. The synoptic-scale activity is strongly reduced (-2hPa) over the North Atlantic and enhanced (1.5hPa) over the South Atlantic and Southern Europe and associated with the negative phase of the NAO and a reduced zonal flow.

The negative NAO pattern also occurs more frequently in March following low Arctic sea ice conditions in ERA-Interim and AFES. The related synoptic-scale patterns differ only slightly from those in February. However, the positive temperature anomalies over the Chukchi Sea nearly vanish because of less cold advection from Siberia. Anomalies in other areas are slightly reduced, which may be interpreted as a weakened influence of sea ice conditions on the circulation patterns and the related temperature anomalies. In March, other processes such as heating of the land masses influence temperatures. However, the synoptic-scale activity anomalies do hardly differ from those in February.

The AFES simulations reveal not only a more frequent occurrence of the NAO-, but also a more frequent occurrence of the NAO + pattern. The sea-ice reduction potentially acts as an additional external forcing to the atmosphere resulting in a generally intensified dominance and intensified variability of the NAO teleconnection pattern. It seems plausible, that the missing preconditioning of the stratospheric vortex due to the missing snow-initiated stratospheric pathway in the AFES model simulation can explain at least partly why the NAO- response in the model is weaker.

5. Conclusions

In this study, we analyzed the preferred atmospheric circulation patterns over the North-Atlantic-Eurasian region and the related 2 m temperature and synoptic-scale activity patterns and investigated changes in their frequency of occurrence for periods with low Arctic sea ice conditions using ERA-Interim reanalysis and AFES model simulations. Hints from literature studies indicate that there is a temporal evolution of pathways and feedback processes between the troposphere and stratosphere from autumn to late winter. In contrast to most previous studies, we therefore analyzed the monthly evolution of synoptic patterns from December to March related to preferred large-scale patterns occurring more frequently during low sea ice conditions.

We showed that the preferred circulation patterns, which occur more frequently in periods with low Arctic sea ice conditions from autumn to winter are an enhanced Scandinavian blocking with negative SLP anomalies over Greenland in December and January and a negative NAO pattern in February and March. The related 2 m temperature patterns in December showed positive anomalies of 1–6 K over Greenland and the Barents, Kara and Laptev Seas as well as negative anomalies of up to −8 K over Siberia. The cyclonic activity over Greenland and the Barents Sea is increased by about 30% and transports more warm air into the Arctic. The same applies in January. Accordingly, the maximum anomalous temperature signal over Svalbard is strengthened.

In February and March, the related synoptic patterns reveal a southward shift of the Atlantic storm track connected with negative temperature anomalies of up to −6 K over Scandinavia, the BKS and Siberia and positive anomalies over the Baffin Bay and Greenland.

In general, ERA-Interim and AFES agreed well on the preferred atmospheric circulation patterns and showed the same temporal evolution of synoptic patterns from December to March. This emphasizes the role of the Arctic sea ice loss in forcing changes in frequency of occurrence of preferred atmospheric circulation regimes. The dynamical reasons for the temporal evolution of synoptic patterns from December to March involve synoptic-planetary wave interaction processes and tropo-stratospheric interaction processes. Thus, the good agreement between ERA-Interim and AFES also emphasizes, that the model is able to simulate these processes reasonably well. On the other hand, the differences in the results between ERA-Interim and AFES provide valuable information on potential areas for model improvement. In particular we suggest that a realistic representation of snow cover over land areas could lead to more realistic simulation of feedback processes initiated by snow cover changes. Furthermore, anomalous warming/cooling over regions outside the Arctic region can provide wave sources for planetary wave trains and have to be taken into account in future studies.

All in all, we conclude that the detected changes in the frequency of occurrence of large-scale circulation patterns can be associated with changes in Arctic sea ice conditions.

Acknowledgements

The authors thank Sabine Erxleben for supporting us with the data analyses. This study has been supported by the project QUARCCS “QUAntifying Rapid Climate Change in the Arctic: regional feedbackS and large-scale impacts” funded by the German Federal Ministry for Education and Research (BMBF) under grant agreement 03F0777A. TN, KY, JU are in part supported by the Arctic Challenge for Sustainability Project (ArCS) and the Belmont Forum InterDec Project. We also thank the AFES development team at the Japan Agency for Marine-Earth Science and Technology, at which the AFES simulations were performed using the Earth Simulator.

Appendix A

Supplementary data related to this article can be found at http://dx.doi.org/10.1016/j.polar.2017.09.002.

References

Alexander, M.A., Bhatt, U.S., Walsh, J.E., Timlin, M.S., Miller, J.S., Scott, J.D., 2004. The atmospheric response to realistic Arctic sea ice anomalies in an AGCM during winter. J. Clim. 17 (5), 890–905. http://dx.doi.org/10.1175/1520-0442(2004)017<0890:TARTRA>2.0.CO;2.

Barnston, A.G., Livezey, R.E., 1987. Classification, seasonality and persistence of low-frequency atmospheric circulation patterns. Mon. Wea. Rev. 115 (6), 1083–1126.

Blackmon, M.L., 1976. A climatological spectral study of the 500 mb geopotential height of the Northern Hemisphere. J. Atmos. Sci. 33 (8), 1607–1623. http://dx.doi.org/10.1175/1520-0469(1976)033<1607:ACSSOT>2.0.CO;2.

Bueh, C., Nakamura, H., 2007. Scandinavian pattern and its climatic impact. Quart. J. Roy. Meteor. Soc. 133 (629, Part B), 2117–2131. http://dx.doi.org/10.1002/qj.173.

Cheung, H.N., Zhou, W., Mok, H.Y., Wu, M.C., 2012. Relationship between ural-siberian blocking and the East asian winter monsoon in relation to the arctic oscillation and the El nino-southern oscillation. J. Clim. 25 (12), 4242–4257. http://dx.doi.org/10.1175/JCLI-D-11-00225.1.

Cheung, H.N., Zhou, W., Shao, Y., Chen, W., Mok, H.Y., Wu, M.Ch, 2013. Observational climatology and characteristics of wintertime atmospheric blocking over Ural-Siberia. Clim. Dyn. 41 (1, SI), 63–79. http://dx.doi.org/10.1007/s00382-012-1587-6.

Christiansen, B., 2007. Atmospheric circulation regimes: can cluster analysis provide the number? J. Clim. 20 (10), 2229–2250. http://dx.doi.org/10.1175/JCLI4107.1.

Cohen, J., Barlow, M., Kushner, P.J., Saito, K., 2007. Stratosphere-troposphere coupling and links with Eurasian land surface variability. J. Clim. 20 (21), 5335–5343. http://dx.doi.org/10.1175/2007JCLI1725.1.

Cohen, J.L., Furtado, J.C., Barlow, M.A., Alexeev, V.A., Cherry, J.E., 2012. Arctic warming, increasing snow cover and widespread boreal winter cooling. Environ. Res. Lett. 7 (1), 014007. http://dx.doi.org/10.1088/1748-9326/7/1/014007.

Cohen, J., Screen, J.A., Furtado, J.C., Barlow, M., Whittleston, D., Coumou, D., Francis, J., Dethloff, K., Entekhabi, D., Overland, J., Jones, J., 2014. Recent Arctic amplification and extreme mid-latitude weather. Nat. Geosci. 7 (9), 627–637. http://dx.doi.org/10.1038/ngeo2234.

Dawson, A., Palmer, T.N., Corti, S., 2012. Simulating regime structures in weather and climate prediction models. Geophys. Res. Lett. 39 (21), L21805. http://dx.doi.org/10.1029/2012GL053284.

Dawson, A., Palmer, T.N., 2015. Simulating weather regimes: impact of model resolution and stochastic parameterization. Clim. Dyn. 44 (7–8), 2177–2193. http://dx.doi.org/10.1007/s00382-014-2238-x.

Dee, D.P., Uppala, S.M., Simmons, A.J., Berrisford, P., Poli, P., Kobayashi, S., Andrae, U., Balmaseda, M.A., Balsamo, G., Bauer, P., Bechtold, P., Beljaars, A.C.M., van de Berg, L., Bidlot, J., Bormann, N., Delsol, C., Dragani, R., Fuentes, M., Geer, A.J.,

Haimberger, L., Healy, S.B., Hersbach, H., Holm, E.V., Isaksen, L., Kallberg, P., Koehler, M., Matricardi, M., McNally, A.P., Monge-Sanz, B.M., Morcrette, J.-J., Park, B.-K., Peubey, C., de Rosnay, P., Tavolato, C., Thepaut, J.-N., Vitart, F., 2011. The ERA-Interim reanalysis: configuration and performance of the data assimilation system. Q. J. R. Meteorol. Soc. 137 (656), 553–597. http://dx.doi.org/10.1002/qj.828.

Deser, C., Phillips, A.S., 2009. Atmospheric circulation trends, 1950–2000: the relative roles of sea surface temperature forcing and direct atmospheric radiative forcing. J. Clim. 22 (2), 396–413. http://dx.doi.org/10.1175/2008JCLI2453.1.

Fetterer, F., Knowles, K., 2004. Sea ice index monitors polar ice extent. EOS Trans. Am. Geo. U. 85 (16) http://dx.doi.org/10.1029/2004EO160007, 163–163.

Francis, J.A., Chan, W., Leathers, D.J., Miller, J.R., Veron, D.E., 2009. Winter Northern Hemisphere weather patterns remember summer Arctic sea-ice extent. Geophys. Res. Lett. 36 (7), L07503. http://dx.doi.org/10.1029/2009GL037274.

Francis, J.A., Vavrus, S.J., 2012. Evidence linking Arctic amplification to extreme weather in mid-latitudes. Geophys. Res. Lett. 39 (6), L06801. http://dx.doi.org/10.1029/2012GL051000.

García-Serrano, J., Frankignoul, C., King, M.P., Arribas, A., Gao, Y., Guemas, V., Matei, D., Msadek, R., Park, W., Sanchez-Gomez, E., 2016. Multi-model assessment of linkages between eastern Arctic sea-ice variability and the Euro-Atlantic atmospheric circulation in current climate. Clim. Dyn. http://dx.doi.org/10.1007/s00382-016-3454-3.

Gastineau, G., García-Serrano, J., Frankignoul, C., 2017. The influence of autumnal Eurasian snow cover on climate and its link with Arctic sea ice cover. J. Clim. 2017 Jun 21. http://dx.doi.org/10.1175/jcli-d-16–0623.1 [early online release].

Handorf, D., Dethloff, K., Marshall, A.G., Lynch, A., 2009. Climate regime variability for past and present time slices simulated by the Fast Ocean Atmosphere Model. J. Clim. 22 (1), 58–70. http://dx.doi.org/10.1175/2008JCLI2258.1.

Hannachi, A., Straus, D.M., Franzke, C.L., Corti, S., Woollings, T., 2017. Low frequency nonlinearity and regime behavior in the northern Hemisphere extra-tropical atmosphere. Rev. Geophys. 55, 36. http://dx.doi.org/10.1002/2015RG000509.

Honda, M., Inoue, J., Yamane, S., 2009. Influence of low Arctic sea-ice minima on anomalously cold Eurasian winters. Geophys. Res. Lett. 36 (8), L08707. http://dx.doi.org/10.1029/2008GL037079.

Hoskins, B.J., Karoly, D.J., 1981. The steady linear response of a spherical atmosphere to thermal and orographic forcing. J. Atmos. Sci. 38 (6), 1179–1196. http://dx.doi.org/10.1175/1520-0469(1981)038<1179:TSLROA>2.0.CO;2.

Hurrell, J.W., Hack, J.J., Shea, D., Caron, J.M., Rosinski, J., 2008. A new sea surface temperature and sea ice boundary dataset for the Community Atmosphere Model. J. Clim. 21 (19), 5145–5153. http://dx.doi.org/10.1175/2008JCLI2292.1.

Inoue, J., Hori, M.E., Takaya, K., 2012. The role of Barents Sea ice in the wintertime cyclone track and emergence of a warm-Arctic cold-Siberian anomaly. J. Clim. 25 (7), 2561–2568. http://dx.doi.org/10.1175/JCLI-D-11-00449.1.

Jaiser, R., Dethloff, K., Handorf, D., Rinke, A., Cohen, J., 2012. Impact of sea ice cover changes on the Northern Hemisphere atmospheric winter circulation. Tellus A 64, 11595. http://dx.doi.org/10.3402/tellusa.v64i0.11595.

Jung, O., Sung, M.K., Sato, K., Lim, Y.K., Kim, S.J., Baek, E.H., Jeong, J.H., Kim, B.M., 2017. How does the SST variability over the western North atlantic ocean control arctic warming over the barents-kara seas? Environ. Res. Lett. 12 (3) http://dx.doi.org/10.1088/1748-9326/aa5f3b.

Jaiser, R., Nakamura, T., Handorf, D., Dethloff, K., Ukita, J., Yamazaki, K., 2016. Atmospheric winter response to Arctic sea ice changes in reanalysis data and model simulations. J. Geophys. Res. 121 (13), 7564–7577. http://dx.doi.org/10.1002/2015JD024679.

Kageyama, M., D'andrea, F., Ramstein, G., Valdes, P.J., Vautard, R., 1999. Weather regimes in past climate atmospheric general circulation model simulations. Clim. Dyn. 15 (10), 773–793. http://dx.doi.org/10.1007/s003820050315.

Kim, B.M., Son, S.W., Min, S.K., Jeong, J.H., Kim, S.J., Zhang, X., Shim, T., Yoon, J.H., 2014. Weakening of the stratospheric polar vortex by Arctic sea-ice loss. Nat. Commun. 5 http://dx.doi.org/10.1038/ncomms5646.

Liu, J., Curry, J.A., Wang, H., Song, M., Horton, R.M., 2012. Impact of declining Arctic sea ice on winter snowfall. Proc. Natl. Acad. Sci. U. S. A. 109 (11), 4074–4079. http://dx.doi.org/10.1073/pnas.1114910109.

Luo, D., Xiao, Y., Yao, Y., Dai, A., Simmonds, I., Franzke, C.L.E., 2016. Impact of ural blocking on winter warm arctic-cold Eurasian anomalies. Part I: blocking-induced amplification. J. Clim. 29 (11), 3925–3947. http://dx.doi.org/10.1175/JCLI-D-15-0611.1.

Luo, D., Yao, Y., Dai, A., Simmonds, I., Zhong, L., 2017. Increased quasi stationarity and persistence of winter ural blocking and Eurasian extreme cold Events in response to arctic warming. Part II: a theoretical Explanation. J. Clim. 30 (10), 3569–3587. http://dx.doi.org/10.1175/JCLI-D-16-0262.1.

Maturilli, M., Kayser, M., 2016. Arctic warming, moisture increase and circulation changes observed in the Ny-Ålesund homogenized radiosonde record. Theor. Appl. Climatol. 17. http://dx.doi.org/10.1007/s00704-016-1864-0.

Michelangeli, P.A., Vautard, R., Legras, B., 1995. Weather regimes: recurrence and quasi stationarity. J. Atmos. Sci. 52 (8), 1237–1256. http://dx.doi.org/10.1175/1520-0469(1995)052<1237:WRRAQS>2.0.CO;2.

Mo, K., Ghil, M., 1988. Cluster analysis of multiple planetary flow regimes. J. Geophys. Res. 93 (D9), 10927–10952. http://dx.doi.org/10.1029/JD093iD09p10927.

Mori, M., Watanabe, M., Shiogama, H., Inoue, J., Kimoto, M., 2014. Robust Arctic sea-ice influence on the frequent Eurasian cold winters in past decades. Nat. Geosci. 7 (12), 869–873. http://dx.doi.org/10.1038/NGEO2277.

Nakamura, T., Yamazaki, K., Iwamoto, K., Honda, M., Miyoshi, Y., Ogawa, Y., Ukita, J., 2015. A negative phase shift of the winter AO/NAO due to the recent Arctic sea-ice reduction in late autumn. J. Geophys. Res. 120 (8), 3209–3227. http://dx.doi.org/10.1002/2F2014JD022848.

Nakamura, T., Yamazaki, K., Iwamoto, K., Honda, M., Miyoshi, Y., Ogawa, Y., Tomikawa, Y., Ukita, J., 2016. The stratospheric pathway for Arctic impacts on mid-latitude climate. Geophys. Res. Lett. 43, 3494–3501. http://dx.doi.org/10.1002/2016GL068330.

Orsolini, Y.J., Senan, R., Vitart, F., Balsamo, G., Weisheimer, A., Doblas-Reyes, F.J., 2016. Influence of the Eurasian snow on the negative North Atlantic Oscillation in subseasonal forecasts of the cold winter 2009/2010. Clim. Dyn. 47 (3–4), 1325–1334. http://dx.doi.org/10.1007/s00382-015-2903-8.

Overland, J.E., Wang, M., 2010. Large-scale atmospheric circulation changes are associated with the recent loss of Arctic sea ice. Tellus A 62 (1), 1–9. http://dx.doi.org/10.1111/j.1600-0870.2009.00421.x.

Overland, J., Francis, J.A., Hall, R., Hanna, E., Kim, S.J., Vihma, T., 2015. The melting Arctic and midlatitude weather patterns: are they connected? J. Clim. 28 (20), 7917–7932. http://dx.doi.org/10.1175/JCLI-D-14-00822.1.

Overland, J.E., 2016. A difficult Arctic science issue: midlatitude weather linkages. Polar Sci. 10 (3), 210–216. http://dx.doi.org/10.1016/j.polar.2016.04.011.

Palmer, T.N., 1993. Extended-range atmospheric prediction and the Lorenz model. B. Am. Meteorol. Soc. 74 (1), 49–65. http://dx.doi.org/10.1175/1520-0477(1993)074<0049:ERAPAT>2.0.CO;2.

Palmer, T.N., 1999. A nonlinear dynamical perspective on climate prediction. J. Clim. 12 (2), 575–591. http://dx.doi.org/10.1175/1520-0442(1999)012<0575:ANDPOC>2.0.CO;2.

Petoukhov, V., Semenov, V.A., 2010. A link between reduced Barents-Kara sea ice and cold winter extremes over northern continents. J. Geophys. Res. 115 (D21), D21111. http://dx.doi.org/10.1029/2009JD013568.

R Core Team, 2012. R: a Language and Environment for Statistical Computing. R Foundation for Statistical Computing, Vienna, Austria. ISBN 3-900051-07-0. http://www.R-project.org/.

Sato, K., Inoue, J., Watanabe, M., 2014. Influence of the Gulf stream on the Barents sea ice retreat and Eurasian coldness during early winter. Environ. Res. Lett. 9 (8) http://dx.doi.org/10.1088/1748-9326/9/8/084009.

Screen, J.A., Simmonds, I., 2010. The central role of diminishing sea ice in recent Arctic temperature amplification. Nature 464 (7293), 1334–1337. http://dx.doi.org/10.1038/nature09051.

Semmler, T., Stulic, L., Jung, T., Tilinina, N., Campos, C., Gulev, S., Koracin, D., 2016. Seasonal atmospheric responses to reduced Arctic sea ice in an ensemble of coupled model simulations. J. Clim. 29 (16), 5893–5913. http://dx.doi.org/10.1175/JCLI-D-15-0586.1.

Smoliak, B.V., Wallace, J.M., 2015. On the leading patterns of northern Hemisphere sea level pressure variability. J. Atmos. Sci. 72 (9), 3469–3486. http://dx.doi.org/10.1175/JAS-D-14-0371.1.

Stephenson, D.B., Hannachi, A., O'Neill, A., 2004. On the existence of multiple climate regimes. Q. J. R. Meteorol. Soc. 130 (597), 583–605. http://dx.doi.org/10.1256/qj.02.146.

Straus, D.M., Corti, S., Molteni, F., 2007. Circulation regimes: chaotic variability versus SST-forced predictability. J. Clim. 20 (10), 2251–2272. http://dx.doi.org/10.1175/JCLI4070.1.

Stroeve, J.C., Maslanik, J., Serreze, M.C., Rigor, I., Meier, W., Fowler, C., 2011. Sea ice response to an extreme negative phase of the Arctic Oscillation during winter 2009/2010. Geophys. Res. Lett. 38 (2), L02502. http://dx.doi.org/10.1029/2010GL045662.

Takaya, K., Nakamura, H., 2005a. Mechanisms of intraseasonal amplification of the cold Siberian high. J. Atmos. Sci. 62 (12), 4423–4440. http://dx.doi.org/10.1175/JAS3629.1.

Takaya, K., Nakamura, H., 2005b. Geographical dependence of upper-level blocking formation associated with intraseasonal amplification of the Siberian high. J. Atmos. Sci. 62 (12), 4441–4449. http://dx.doi.org/10.1175/JAS3628.1.

Vihma, T., 2014. Effects of Arctic sea ice decline on weather and climate: a review. Surv. Geophys. 35 (5), 1175–1214. http://dx.doi.org/10.1007/s10712-014-9284-0.

Wegmann, M., Orsolini, Y., Vázquez, M., Gimeno, L., Nieto, R., Bulygina, O., Jaiser, R., Handorf, D., Rinke, A., Dethloff, K., Sterin, A., Brönnimann, S., 2015. Arctic moisture source for Eurasian snow cover variations in autumn. Environ. Res. Lett. 10 (5), 054015. http://dx.doi.org/10.1088/1748-9326/10/5/054015.

Yang, X.Y., Yuan, X., Ting, M., 2016. Dynamical link between the barents-kara sea ice and the arctic oscillation. J. Clim. 29 (14), 5103–5122. http://dx.doi.org/10.1175/JCLI-D-15-0669.1.